Jour. Fac. Sci., Hokkaido Univ., Ser. VII (Geophysics), Vol. 11, No. 2, 441-460, 1998.

Preliminary Results of a Global High-Resolution GCM Experiment

Akio Ishida, Yuji Kashino, Humio Mitsudera*

Japan Marine Science and Technology Center, 2-15, Natsushima-cho, Yokosuka 237-0061, Japan

Noriya Yoshioka

Japan Meteological Agency, 1-3-4, Otemachi, Chiyoda-ku 100-0004, Japan

and

Teruaki Kadokura

Fuji Research Institute Corp, Takezono Square, Kanda Nishi-cho, Chiyoda-ku 101-0054, Japan

(Received November 30, 1997)

Abstract

To examine the role of the meso-scale eddies in the ocean general circulation, we have investigated the circulation which is simulated by a high resolution general circulation model with 1/4 degrees grid spacing and 55 vertical levels. The model in this study simulates quite well the Kuroshio and its separation, and the equatorial currents system comprising the Equatorial Undercurrent and Subsurface Countercurrent, etc., which have not been well reproduced in previous models. The model also shows the characteristics of fluctuations known on the basis of observation, such as latitudinal dependence of the westward phase speed of the Rossby wave and fluctuations of the Indonesian throughflow. We describe the mean and eddy characteristics in the model compared with observed results, and discuss the role of the meso-scale eddies in the ocean general circulation.

1. Introduction

The ocean circulation in surface and subsurface layers should be understood in order to predict interannual to decadal climate variability, because it plays an important role in heat transport in the subtropical and subarctic areas. In most

* Present affiliation: International Pacific Research Center, SOEST, University of Hawaii, 1000 Pope Road, Honolulu, Hawaii 96822, U.S.A.

previous numerical studies, coarse resolution (about 1 to 4 degrees horizontally) general circulation models (GCM), in which small scale phenomena such as mixing by meso-scale eddies are parameterized, have been used. The greatest concern in such studies is how to simulate the real ocean circulation by tuning many parameters. No model can simulate the real ocean circulation satisfactorily to date. Moreover, even if the observed results are simulated by some models, they will not be useful for climate prediction until the mechanism of the ocean circulation is well understood.

Therefore, the role of the meso-scale eddies in the general circulation should be investigated with a high-resolution model in which eddies are explicitly resolved instead of parameterized. Regional models with high-resolution may be used to investigate the meso-scale phenomena to basin scale circulation, but not to investigate the interocean exchanges, such as the deep water spreading out from the North Atlantic to the Pacific and Indian Oceans, and the Indonesian Throughflow, which are investigated in oceanography because of the relationship on to climate variability. As mentioned above, a global high-resolution model is needed to understand the role of ocean in climate variability ; however, few such models have been developed until recently because of limited computer resources.

The purpose of this study is to understand the role of the meso-scale eddies in the general circulation, and the mechanism of seasonal to annual variability, by investigating the behavior of the ocean circulation obtained with a global high-resolution model. The model ocean is spun up with annual averaged climatological surface boundary conditions, and then forced by monthly averaged conditions to investigate the seasonal variability. In this paper, we introduce the results in the model for 10 years as preliminary results.

2. Model description

The model in this study is based on the Modular Ocean Model version 2 (MOM2) developed at the NOAA Geophysical Fluid Dynamics Laboratory (GFDL) (Pacanowski, 1995). One of the advantages of using MOM2 is that the model is widely used throughout the world and it is easy to make comparisons among the results of various studies with MOM2. Another advantage is that the implementation of new schemes and parameterizations constructed by many modelers has been performed in GFDL.

The global high-resolution model by Semtner and Chervin (1988, 1992) could not simulate well the separation of the Kuroshio and the Gulf Stream, and the

Table 1. Depths of Model Levels. ZT corresponds to the depth of temperature, salinity and horizontal velocities. ZW corresponds the depth of vertical velocity.

Level	ZT (m)	ZW (m)	Level	ZT (m)	ZW (m)	Level	ZT (m)	ZW (m)
1	5.00	10.00	20	343.78	363.78	38	1,435.26	1,479.39
2	15.00	20.00	21	383.78	405.35	39	1,523.52	1,574.51
3	25.00	30.00	22	426.92	450.04	40	1,625.51	1,685.04
4	35.00	40.00	23	473.16	497.79	41	1,744.57	1,814.09
5	45.00	50.00	24	522.43	548.53	42	1,883.61	1,964.34
6	55.00	60.08	25	574.63	602.13	43	2,045.07	2,137.94
7	65.16	70.49	26	629.63	658.45	44	2,230.81	2,336.46
8	75.82	81.55	27	687.26	717.30	45	2,442.11	2,560.86
9	87.29	93.59	28	747.34	778.48	46	2,679.61	2,811.46
10	99.88	106.89	29	809.63	841.77	47	2,943.31	3,087.94
11	113.90	121.77	30	873.90	906.89	48	3,232.57	3,389.34
12	129.63	138.48	31	939.88	973.59	49	3,546.11	3,714.09
13	147.34	157.30	32	1,007.29	1,041.55	50	3,882.07	4,060.04
14	167.26	178.45	33	1,075.82	1,110.49	51	4,238.01	4,424.51
15	189.63	202.13	34	1,145.16	1,180.08	52	4,611.02	4,804.39
16	214.63	228.53	35	1,215.00	1,250.00	53	4,997.76	5,196.16
17	242.43	257.79	36	1,285.00	1,321.03	54	5,394.56	5,596.03
18	273.16	290.04	37	1,357.06	1,396.16	55	5,797.50	6,000.00
19	306.92	325.35						

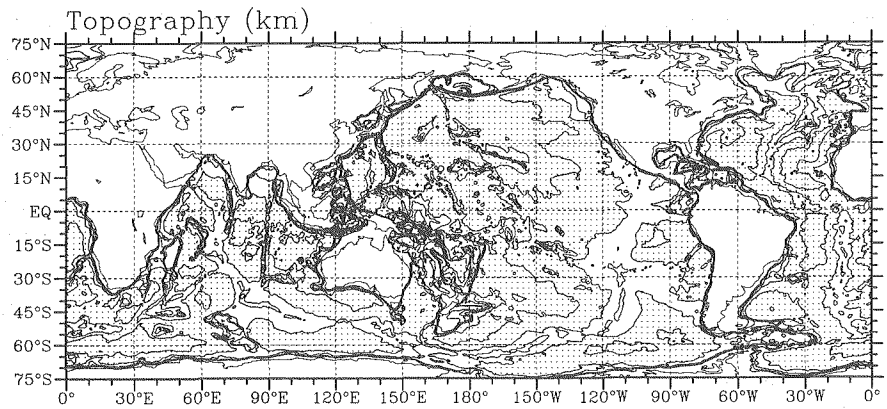

Fig. 1. Model geometry with a contour interval of 1 km. Depths less than 4 km are shaded.

vertical structure of zonal currents in the equatorial region. We think that one of the reasons is that the vertical resolution of their model (20 levels) is not high enough to simulate those phenomena. Therefore, the model used for this study has nearly three times as high a vertical resolution as that of Semtner and Chervin (1988, 1992). There are 55 levels in the vertical, with a spacing of 10 m at the surface, smoothly stretching to 50 m in the intermediate layer and to about 400 m by 6,000 m (Table 1). The horizontal resolution is 1/4 degrees in both latitude and longitude. The model covers the global ocean from 75°S to 75°N except the Arctic Ocean.

The model topography is derived from NOAA National Geophysical Data Center dataset (ETOPO5) with 5′ latitude-longitude resolution. Because the original topography from ETOPO5 is too steep, the Gaussian spatial smoother with the influence radii of 0.5 degrees (about 50 km at the equator) above 1,000 m depth, and smoothly increasing to 1 degree at 6,000 m depth, is applied for the original topography. Additionally, it is checked and modified to remove single gridpoint holes or spikes and small islands. The model geometry is shown in Fig. 1.

The model is driven from the initial state at rest with annual averaged temperature and salinity of Levitus (1982) climatology. The surface boundary conditions are all based on climatological datasets. The heat and freshwater flux are implemented as a linear restoring of temperature and salinity in the first model level toward Levitus (1982) data. The restoring timescale is 6 days, which is such that the water characteristics in the surface mixed layer with 50 m thickness is restored toward the data value in 30 days. The Hellerman and Rosenstein (1983) wind stress data is used to force the model. The linear interpolation is used for temperature and salinity data to the model grids. However, for wind stress, the hyperbolic cubic patch is used to maintain smoothly varying derivatives, for example, the curl of the wind stress.

The model first 2 years is the initial spin-up stage. The annual averaged climatologies for surface boundary conditions and a harmonic operator for the horizontal dissipation mechanism are used in this stage. We start the seasonal variability experiment driven by the monthly climatologies from the last state of the initial spin-up. The horizontal dissipation mechanism is a highly scale-selective, biharmonic operator, and the coefficients are set to -1×10^{19} cm^4 sec^{-1} for both momentum and tracers in the seasonal experiment. The vertical dissipation is handled through the Pacanowski and Philander (1981) formulation. Because it is impossible to integrate the equations for a long enough time to spin up the deep ocean due to the short time step for the fine horizontal grids scale,

the restoring terms with the 2 years timescale to the Levitus (1982) climatologies are included in the tracer equations below 2000 m depth. Therefore, the deep layer in this model is robust diagnostic as seen in Sarmiento and Bryan (1982). The time integration has been processed to model 10 years (including the first 2 years). We describe the results mainly from the 9th to 10th model years in the following sections.

3. Kinetic energy

Though the model ocean is being spun up in the model 10th year, the barotropic adjustment has been finished and the meso-scale eddies have been generated in the equatorial and western boundary regions and the area around the Antarctic Circumpolar Current. The time series of kinetic energy in the whole model basin is shown in Fig. 2. The kinetic energy increases drastically within several days from the initial state of zero energy, and decreases until the end of the 2nd year. From the beginning of the 3rd year, it increases again due to the change of the horizontal dissipation mechanism from harmonic to biharmonic operator and the use of the monthly climatologies for surface boundary conditions. After the 5th year, the energy approaches equilibrium, fluctuating

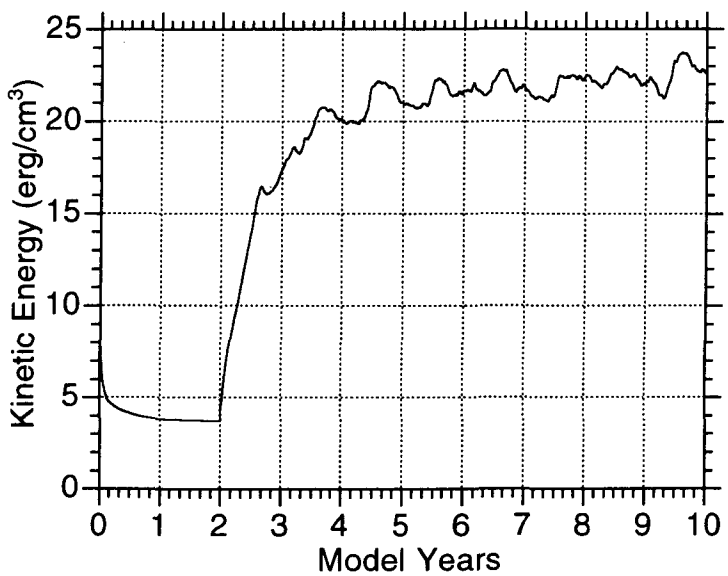

Fig. 2. Time series of global averaged kinetic energy.

from 20 to 25 erg cm^{-3}, which corresponds to a velocity of 6 to 7 cm s^{-1} on the global average, although, as is well known, it is concentrated in the regions with strong currents, such as the western boundary and equatorial regions.

The distributions of the annual mean kinetic energy (MKE) (a) and the eddy kinetic energy (EKE) (b) at the first level (5 m depth) are shown in Fig. 3. The EKE is defined as the energy of flows deviating from the annual mean velocity. These are computed with the results saved every 5 days in the model 10th year. The distribution of the MKE shows large values for the mid-latitude western boundary currents such as the Kuroshio, the Gulf Stream, and the Somali Current in the northern hemisphere, and the East Australian Current, the Brazil Current, and the Agulhas Current in the southern hemisphere. The Kuroshio in this model flows eastward with the large meander off the Kii Peninsula and continues to the Kuroshio Extension with modulation east of the date line after the separation off the Boso Peninsula. The Oyashio flows northeastward along the Subarctic Front from east of the Tsugaru Strait. The structures of the separation and the extension of the Kuroshio derived in this model are consistent with those observed. This suggests that the improvement of the horizontal resolution is effective for the simulation of the Kuroshio structure, because the model with horizontal resolution of 1/2 degrees by Semtner and Chervin (1988, 1992), which is coarser than that of our model, could not simulate the separation of the Kuroshio well. On the other hand, the model Gulf Stream fails to separate from the coast at Cape Hatteras, but rather forms a quasi-permanent eddy north of it. This structure is similar to that in the North Atlantic model (Treguier, 1992) of WOCE CME (World Ocean Circulation Experiment Community Modelling Effort). The resolution of the CME model is 1/3 degrees in latitude and 2/5 degrees in longitude and 30 levels in the vertical. These are lower resolutions than those of the model in this study. As one of the reasons for the failure of the Gulf Stream separation, Treguier (1992) pointed out a lack of inertia of the current due to the insufficient spatial resolution, because the model Florida Current transport was about 25 Sv (1 Sv$=10^6$ m^3s^{-1}), less than the observed 30-31 Sv. Because the transport of this model Florida Current is also about 25 Sv on average, this may be the cause of the problem.

The equatorial region is also energetic as is the mid-latitude western boundary region. The North Equatorial Current flows westward around 10°N in the equatorial North Pacific. This current branches into the northward Phillipine Current and the southward Mindanao Current at the east coast of the Phillipines. The Mindanao Current leads to the Mindanao Eddy, the Halmahera Eddy, and the western route of the Indonesian throughflow. The

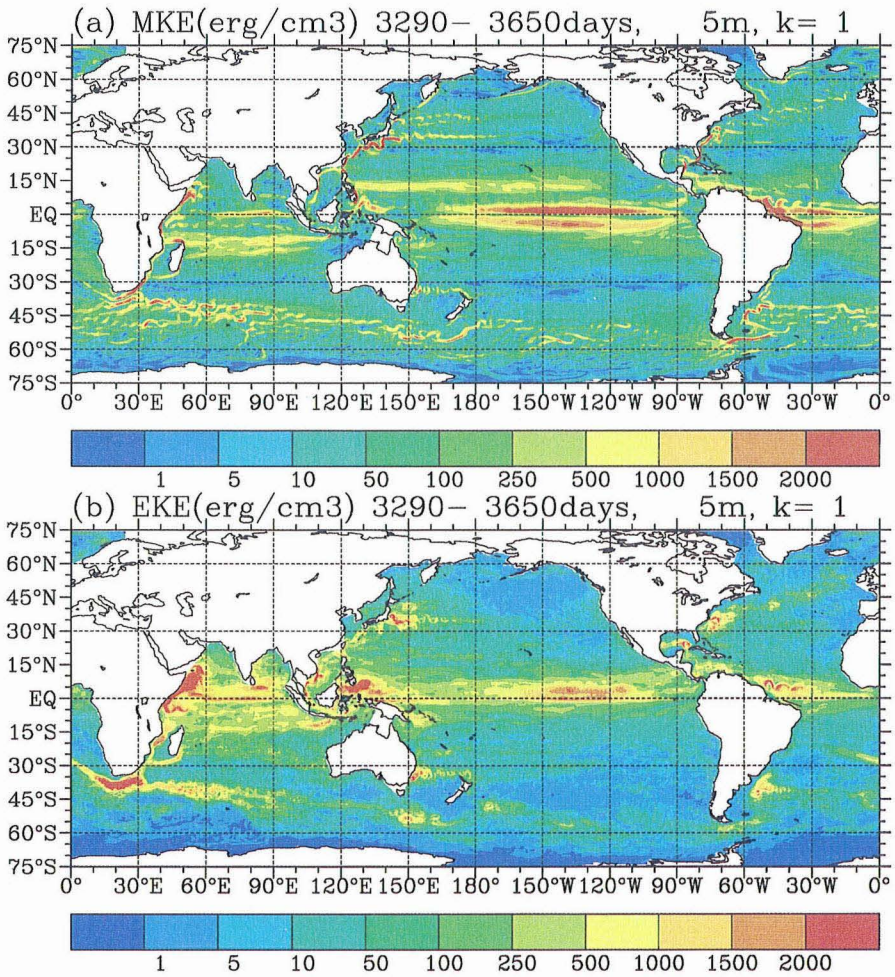

Fig. 3. Distribution of mean kinetic energy (a) and eddy kinetic energy (b) at the first level (5 m depth).

Phillipine Current branches in south of Taiwan into the Kuroshio and the current which flows into the South China Sea. In the Indian Ocean, there is a high energy region comprising the Wyrtki jet along the equator and the South Equatorial Current along 10°S across the Indian Ocean from the Lombok Strait to the Madagascar Island. The South Equatorial Current in the Atlantic has high energy, as it does in the Pacific.

In the Southern Ocean, the current branches into many narrow currents with ridges and sea mounts. Bottom topography seems to influence the energy

distribution in cross stripes. The especially high energy regions are as follows: the south coast of Africa to the Kergelen Plateau in the Indian Ocean sector, the Southeast Indian Ridge to the Pacific-Antarctic Ridge in the western Pacific Ocean sector, and the Drake Passage, the Scotia Sea, and the Argentine Basin in the Atlantic Ocean sector. Bottom topography is very rough in these regions. The directions of the currents' axes correspond to those of the ridges. These distributions suggest a strong influence of the topography on the current structure.

The EKE is also high in the high MKE regions because eddies and meanders are generated due to dynamical instability. The EKE distribution in Fig. 3 (b) shows that the EKE is as high as the MKE in the western boundary regions and the equatorial regions. Because the EKE shown in Fig. 3(b) is defined as the kinetic energy of the deviation from the annual mean velocity, it has components including not only variability with period of the meso-scale eddies but also seasonal one driven by the monthly averaged climatologies. In particular, the EKE in the Indian Ocean is higher than those in the other oceans because of the seasonal variability due to the Indian Monsoon.

In the Pacific, the eddy activity is high around the Kuroshio and the equatorial regions. The high EKE in the Kuroshio region is due to the generation and separation of the Warm and Cold Core Rings and the migration of the Kuroshio Large Meander south of Japan. In the equatorial Pacific, the EKE is high in the western area and east of the date line. The central Pacific from 160°E to the date line does not have high EKE compared with those regions. The source of the high EKE in the eastern equatorial Pacific is the Tropical Instability Waves (e.g., see Legeckis, 1977) with maximum amplitude around 3°N. On the other hand, the source of the EKE in the western equatorial Pacific seems to be the variability of the western boundary currents; thus, the mechanism of the eddy activities in these two regions seem to be different.

In the Atlantic Ocean, the equatorial area has high EKE, similar to the equatorial Pacific. The EKE distribution shows large meanders with 500 km to 1,000 km length. This high EKE seems to be generated by the oscillation of the stationary meanders, not the eddy propagation which is the high EKE mechanism in the eastern Pacific. The peaks of the EKE exist around 5°N and 10°N, not at the equator. It is possible that the effect of coastal geometry in the Atlantic is larger than in the Pacific because the zonal scale of the Atlantic is smaller than that of the Pacific. The eddy activity in the Gulf Stream as well as the Kuroshio is high, but the high EKE region is restricted near the western boundary because the separation is not simulated satisfactorily, as stated above.

The EKE estimated from the Geosat altimeter data (Le Traon et al., 1990) and the drift buoy data (Richardson, 1983) is higher than 1,000 erg cm^{-3}, with the peak around 38°N even in the central Atlantic. The eddy activity in the model central Atlantic is lower than that from observed results.

In the Indian Ocean, the EKE level is high in the equatorial region and the western boundary. This is due to not only the meso-scale variability but also the seasonal variability. The EKE south of Madagascar Island and in the Agulhas Current system is high due to the meso-scale eddies. The vortex streets are clear around the south coast of Africa from the Indian Ocean to the Atlantic Ocean. The activity of the vortices can be followed to 20°W in the South Atlantic.

In the Southern Ocean, the EKE is high in the high MKE regions, the same as for the other oceans, but it is low in the regions south of New Zealand, near the Drake Passage, and the Scotia Sea, where steady currents exist. On the other hand, there are high EKE regions from south of Africa to the Kergelen Plateau, and near the South Tasmania Rise, where many fine branches of the currents exist. These currents branches, due to rough topography, seem to regulate the complex frontal structure along the Antarctic Circumpolar Current.

4. Variability of sea surface height

The sea surface height data from satellites is useful for investigating the global characteristics of ocean variability. Fu and Smith (1996) discussed the characteristics of variability and the model validity, investigating the standard deviations of sea surface height derived from TOPEX/POSEIDON (T/P) data and their high-resolution model results. Their model was developed in the Parallel Ocean Program (POP) in Los-Alamos National Laboratory (Smith et al., 1992) and is a high-resolution model with the averaged horizontal resolution of about 22.2 km or 1/5 degrees. It was forced by the surface wind stress fields from the twice-daily analyses from the European Centre for Medium-Range Weather Forecasts (ECMWF) after a 30 years spin-up computation. The period of their simulation was the same as that for which the T/P data was analyzed (October 1992-October 1994).

Figure 4 shows the standard deviations of the sea surface height derived from T/P data (upper panel), and from the POP model (middle), and the model of this study (lower). We adjust the colors in Fig. 4 (lower) to compare with the POP model and T/P results. Although it is difficult to directly compare our results with theirs because our model is forced by the climatological wind, the

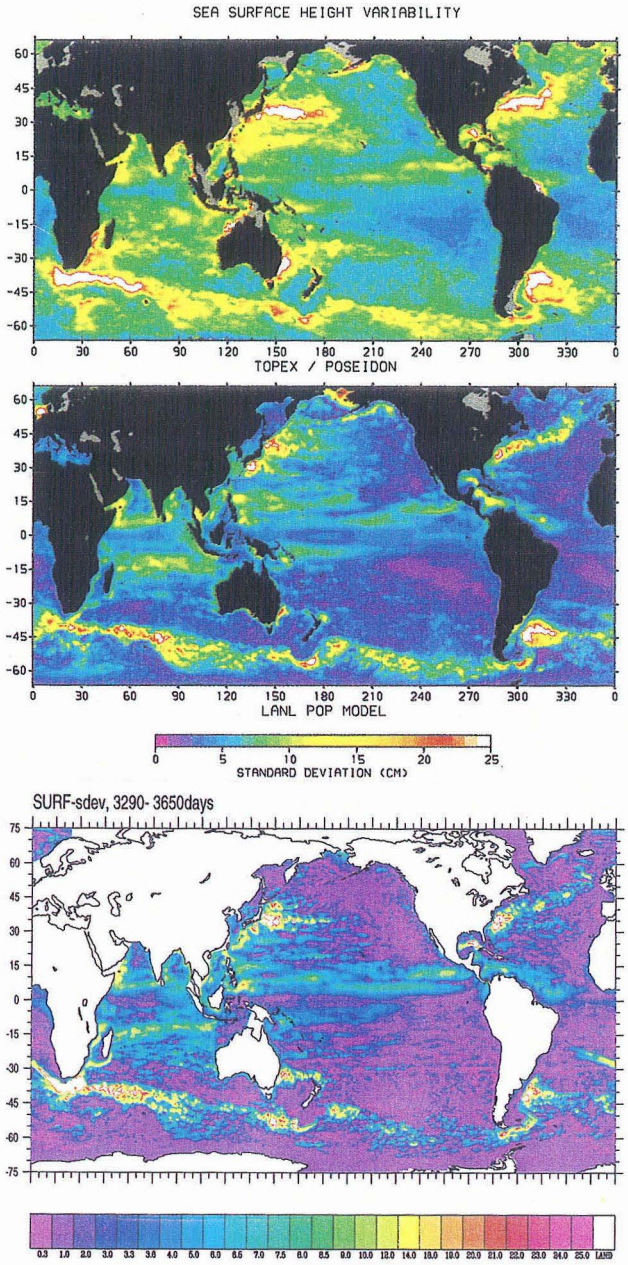

Fig. 4. Standard deviation of the sea surface height. Upper: TOPEX/POSEIDON observation. Middle: the POP model. Lower: this model. The upper and middle panels are from Fu and Smith (1996).

sea surface height from our model agrees with that from T/P as well as the POP model. Of special note, the standard deviation in the Kuroshio Extension, which appears as the eastward extension of the deviation higher than 25 cm shown in Fig. 4, is simulated better by this model than by the POP model. The high vertical resolution of this model is one reason for the better simulation of the Kuroshio separation and the extension, because both the model used in this study and the POP model are based on the GFDL MOM. The structure of the high deviation area in the Agulhas Current region in this model is also more similar to the T/P data than that in the POP model.

Neither the POP model nor this model could represent the distribution of the high variability around 20°N to 25°N in the western Pacific in both hemispheres. Moreover, results from this model indicate that sea surface height variability in the Gulf Stream is small, and its area with high value is confined to the western boundary region of the northern Atlantic because of failure of the Gulf Stream separation. These problems are also reported in the results of the WOCE Parallel Ocean Climate Model (Stammer et al., 1996), developed on the basis of the Semtner and Chervin (1988) model, and should be solved in the present high-resolution GCMs. Furthermore, results from both models show smaller sea surface height variability than that from T/P data in the interior region. However, this may be due to observational errors whose magnitudes are comparable to or larger than those of signals (Fu and Smith, 1996).

5. Propagation of eddies

The variability described in the previous sections is associated with the meso-scale eddies which are generated by dynamic instability and propagate westward due to planetary beta effect and reach western boundaries. Then some of them are reflected, and the rest are dissipated. To examine the propagation speed and spatial scale, we plot the northward velocity anomaly from the annual average at 100 m depth in the model 9th year along the latitudes (equator, 5°N, 10°N, 20°N, 30°N, 40°N) as a function of longitude and time (Fig. 5). The longitudinal range, which covers almost the whole North Pacific, is from 120°E to 80°W. The y-axis is the time in days from Jan 5 to Dec 31 in the model 9th year.

The most prominent feature is the waves in the eastern equatorial area (seen in the plots along the equator and 5°N), which propagate westward with a wavelength of about 1,000 km and a period of about 30 days. The wavelength and the period are consistent with those of the Tropical Instability Waves (i.e.

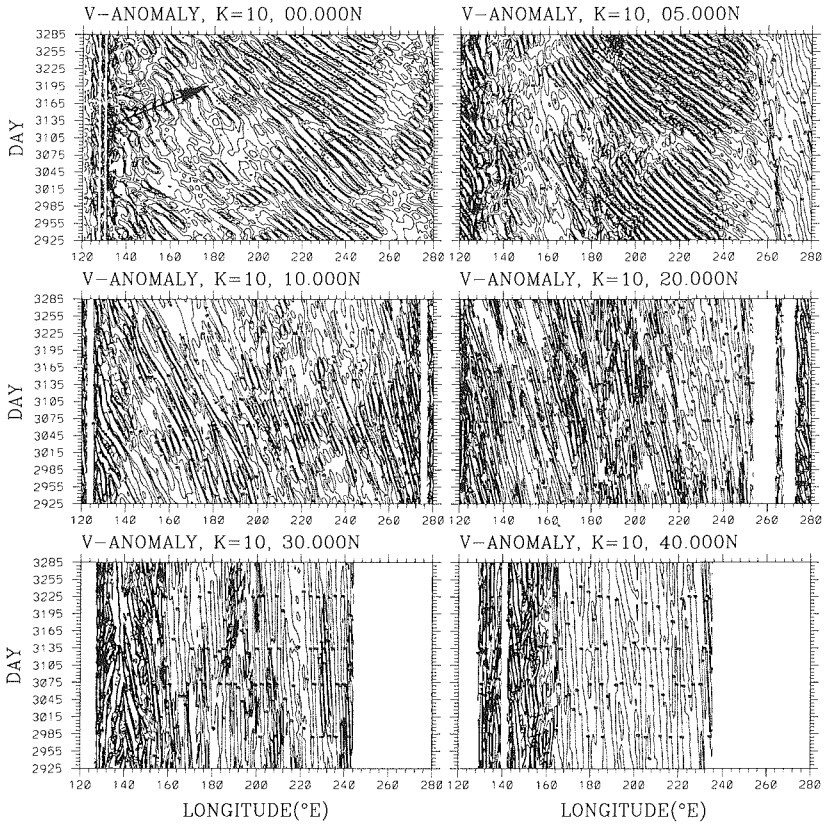

Fig. 5. Northward velocity anomaly (cm s^{-1}) from annual mean as a function of longitude and time at 100 m depth along the latitudes (equator, 5°N, 10°N, 20°N, 30°N, 40°N). The arrow in the top left panel indicates the eastward spreading of the meandering of the equatorial undercurrent stated in the text.

Legeckis, 1977 ; Philander, 1989), and the model simulates well the feature that the wave amplitude is small in April and May (Halpern, 1987). The westward propagation of the waves can be traced around the date line, and the fluctuations in the western Pacific seem to be generated locally, not to be propagated from the east. Large variability is also seen in the western equatorial Pacific ; of special note is the regular westward propagation of perturbations with a wavelength of about 400 km to 500 km and a period of about 40 days in the Sulawesi Sea. They can easily be seen from 120°E to 130°E in the plot for 5°N. In the next section, we describe these fluctuations, which correspond to the westward propagation of eddies detached southeast of Mindanao.

The amplitude of fluctuations in the interior, except the western boundary area, is small and the westward propagation speed becomes small with increasing latitude. The phase speeds taken from the plots are 35-40 cm s^{-1} for the equator and 5°N, 15-20 cm s^{-1} for 10°N, 8-10 cm s^{-1} for 20°N, about 2.5 cm s^{-1} for 30°N, and about 2 cm s^{-1} for 40°N. These values agree closely with the phase speeds of the linear Rossby wave shown in Chelton and Schlax (1996). They indicate that the phase speeds of surface height signals derived from the T/P data are larger than the theoretical Rossby wave phase speeds outside of the tropics. It is important, and left for future work, to compute accurate phase speeds of the waves in the model, and investigate whether the linear Rossby wave theory can be applied to the propagation seen in the model.

6. Mean circulation and variability in the equatorial Pacific

The circulation in the equatorial ocean seems to be steady state in the 10 model years integration because the spin-up time of the equatorial circulation is shorter than that of the mid-latitudes. We describe some topics on the equatorial circulation and variability in the next subsections.

6.1 The oceanic variability in the western equatorial Pacific and the Indonesian throughflow

The Indonesian throughflow is a system of currents flowing from the Pacific Ocean to the Indian Ocean through the Indonesian Seas. It is the only flow between ocean basins at low latitudes and, consequently, plays an important role in the meridional heat transport in the climate system (Meyers, 1996). Although determining the structure and transport of the Indonesian throughflow have been the subjects of increasing attention, they have not yet been elucidated because of a highly complex system of channels and the highly variable nature of currents in the western equatorial Pacific (cf. Lucas et al., 1996 ; Godfrey, 1996). We describe the variability in the Indonesian throughflow region, the relation between the variation in the Sulawesi Sea and that of the Mindanao Eddy, and the clockwise eddy propagating northwestward along the New Guinea Coast, and the growth of the meandering of the Equatorial Undercurrent.

Fluctuations with a period of about 40 days are seen in the Sulawesi Sea (Fig. 5). To examine its horizontal structure, the horizontal velocity vectors at 100 m depth in the throughflow area from 120°E to 150°E, 10°S to 10°N, are drawn with salinity contours (Fig. 6). The plots are shown every 5 days from Jul 19 to Aug. 23 in the model 9th year, and ordered downward from the top left panel

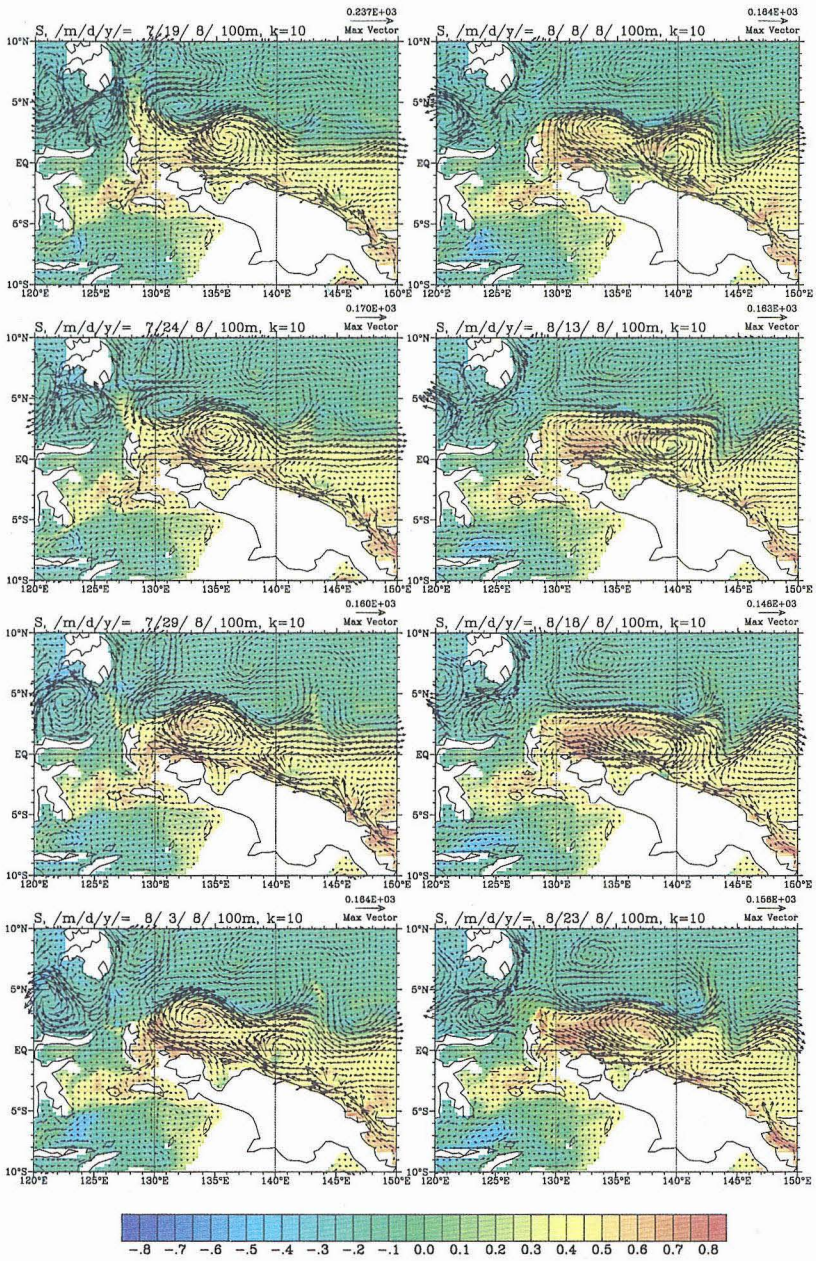

Fig. 6. Horizontal velocity vector overlaid on salinity anomaly from 35 psu distribution at 100 m depth in the western equatorial Pacific. The plots are shown every 5 days from Jul 19 to Aug 23 in the model 9th year and put downward from the top left panel continuing to the right row.

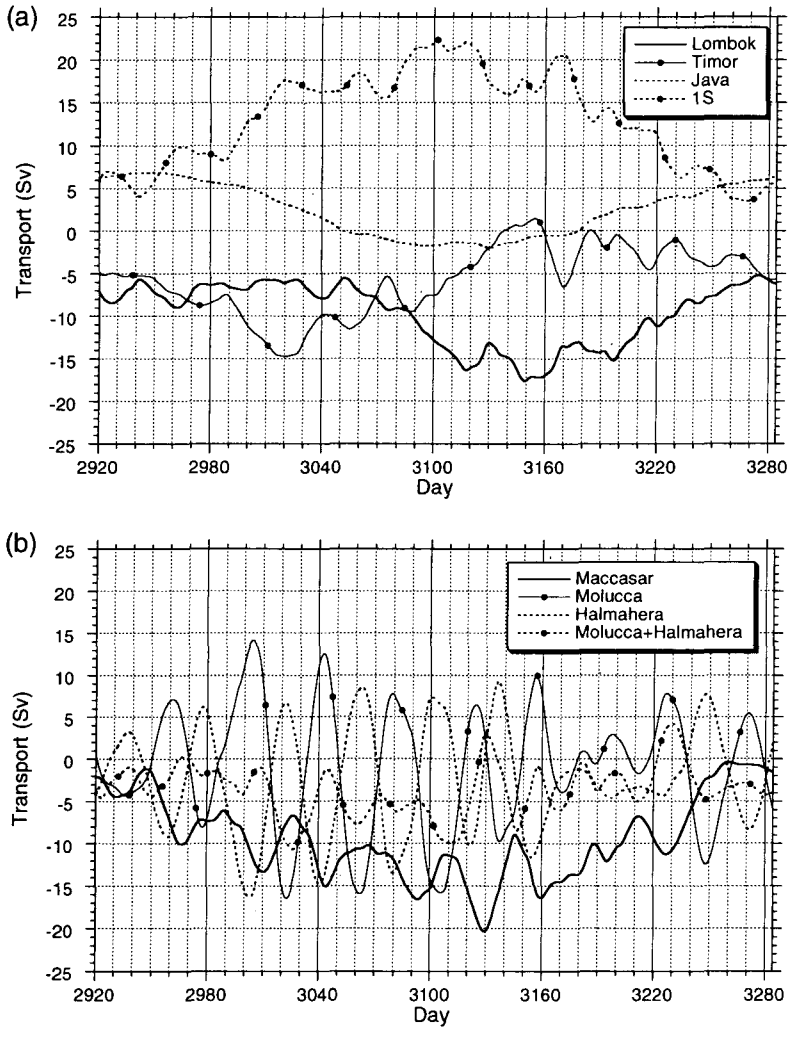

Fig. 7. Time series of the transport of the Indonesian throughflow. (a) Inflow to the Banda Sea. 1S represents the sum of the transports through Makassar Strait, Molucca Strait, and Halmahera Sea. (b) The transports through Makassar Strait, Molucca Strait, and Halmahera Sea. Positive value represents northward. Refer to Fig. 8 for each section.

continuing to the right row. On Jul 19, there are an anti-clockwise eddy with its center at 125°E, 4°N in the Sulawesi Sea, and a clockwise eddy on the west. The anti-clockwise eddy propagates westward and occupies almost the whole

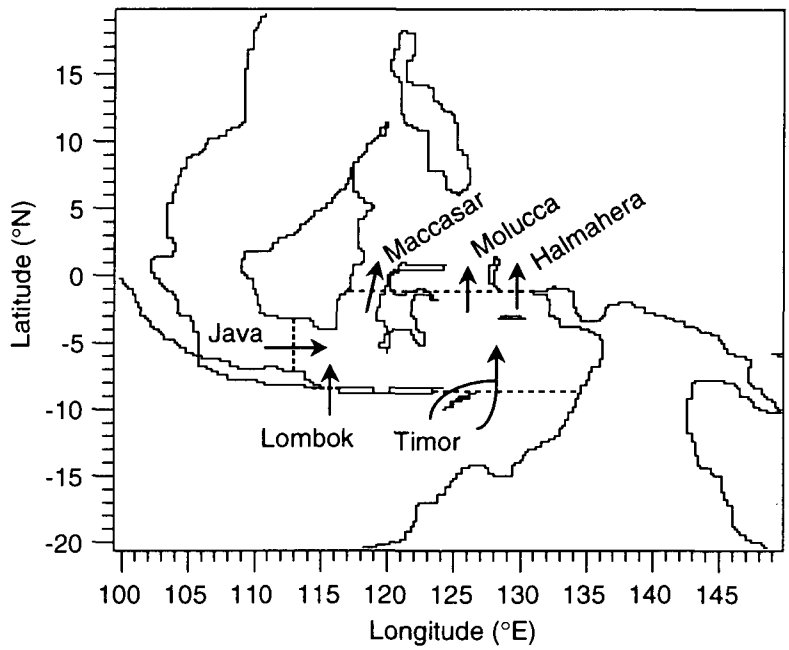

Fig. 8. Sections used to calculate the transport of the Indonesian throughflow shown in Fig. 7.

Sulawesi Sea on Jul 29. At that time, there is another anti-clockwise eddy with its center at 130°E, 5°N. This eddy is located at 127°E on Aug 8, and moves to and occupies the Sulawesi Sea, the same as the previous eddy. The first anti-clockwise eddy has already reached to the western Sulawesi Sea by then, and a small clockwise eddy appears between the two anti-clockwise eddies. After that, the new anti-clockwise eddy propagates westward and it makes a pair of eddies with a clockwise eddy on the west on Aug 18, as on Jul 19.

Such behavior of eddies critically affects the transport of the Indonesian throughflow in this model. Figure 7 shows the transport through the straits shown in Fig. 8. The water from the Pacific to the Banda Sea and the Flores Sea through the Maccasar Strait, Molucca Strait, the Halmahere Sea, and the Java Sea flows out to the Indian Ocean through the Lombok Strait and the Timor Sea. The total transport of the model annual averaged Indonesian throughflow is 15.6 Sv, and the transport through the Lombok Strait is 9.7 Sv. The transport through the Lombok Strait derived in this model is larger than that observed (cf. Arief and Murray, 1996), but the total transport of the model Indonesian throughflow is a plausible value for the real ocean.

The relationship between the behavior of eddies in the Sulawesi Sea and the throughflow transport should be especially noted. Figure 7 (b) shows that the fluctuations of the transports through the Molucca Strait and the Halmahera Sea are out of phase, and both have the same period of about 40 days. It is clear that these fluctuations are related to the propagation of eddies shown in Fig. 6. The period from Jul 19 to Aug 23 in Fig. 6 corresponds to from day 3120 to day 3155 in Fig. 7. When there is an anti-clockwise eddy south of the Mindanao Island in the eastern Sulawesi Sea, there are a northward flow with transport about 5 Sv through the Molucca Strait and a southward flow in the Halmahera Sea from the Pacific to the Banda Sea. Next, the currents through the Molucca Strait and the Halmahera Sea turn around as the eddy propagates westward, and the northward flow through the Halmahera Sea is strengthened on Aug 8 (day 3140). It is found that the characteristics of the water mass into the Banda Sea are influenced by the eddy.

The variability of the New Guinea Coastal Undercurrent (NGCUC) and the development of the meander of the Equatorial Undercurrent (EUC) are interesting phenomena appearing in this model. There is a small clockwise eddy near the New Guinea coast (145°E, 3°S) with low salinity water on Jul 19 in Fig. 6. This eddy enclosing low salinity water is growing with time and propagating northwestward to the equator at 140°E on Aug 3, and then generating a large clockwise circulation concatenated with the Halmahera Eddy west of it. At that time, the EUC flows meandering with a southward flow across the equator at about 142°E. The growth of the meandering of the EUC is also seen in the x-t plot along the equator in Fig. 5, which shows the eastward spreading of the large amplitude of northward velocity anomaly generated in 140°E to 160°E from day 3135 to day 3165 as indicated with a arrow in Fig. 5.

The observed data show variability near the New Guinea coast, as do the model results. Kuroda (1997) reports that 20-30 days perturbation is eminent in the NGCUC, and a 30 days oscillation at the equator, 138°E in the downstream of the NGCUC, is clearly observed from moored ADCP data. He cites the dynamical instability as one cause of this perturbation and suggests that the oscillation is related to the 20-30 days perturbation in the NGCUC. The variations associated with propagation and growth of the eddy in this model may agree with the observed ones.

6.2 *Vertical structure of the water mass and the velocities in the equatorial Pacific*

The model in this study represents quite well the vertical structure of the

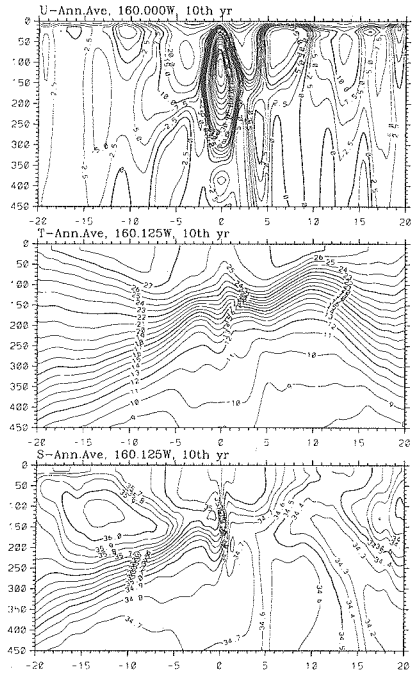

Fig. 9. Annual mean distributions of eastward velocity (upper), temperature (middle), and salinity (lower) in the model 10th year along 160°W.

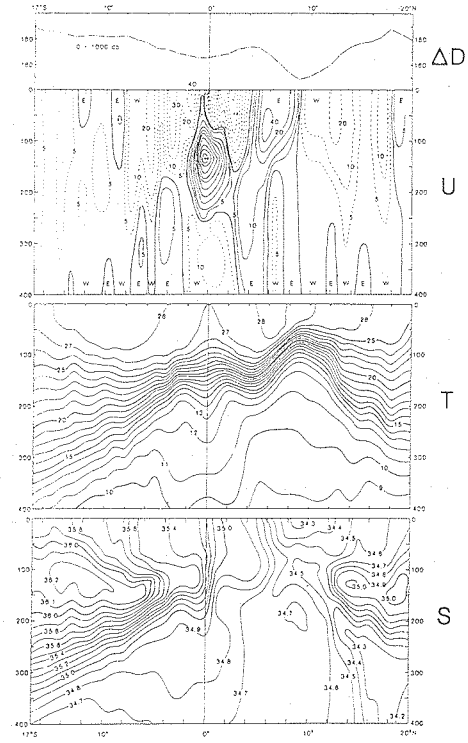

Fig. 10. Mean distributions of dynamic height (△D) relative to 1,000db, eastward geostrophic flow (U), temperature (T), and salinity (S) between Hawaii and Tahiti (Wyrtki and Kilonsky, 1984).

equatorial current system, which could not be simulated in the previous models because of coarse vertical resolution. We show the vertical distributions of the annual averaged eastward velocity, temperature, and salinity in Fig. 9 and those observed in the Hawaii-Tahiti Shuttle Experiment (Wyrtki and Kilonsky, 1984) in Fig. 10. The model simulates the current structure quite well, e.g. the depth as well as the latitudinal positions of the axes of the EUC, the South Equatorial Current, and the North Equatorial Countercurrent. In particular, the westward Equatorial Intermediate Current with the core at the equator, 350 m depth and the Subsurface Counter Currents flowing eastward at 200-300 m depth at latitude 4 degrees are quite well simulated with this model. The water mass distributions, e.g. the shallow, sharp thermocline at 10°N and the salinity front

at the equator, are also well simulated. As mentioned above, this model simulates the equatorial currents system, but the previous models (Semtner and Chervin, 1988, 1992) could not simulate the Equatorial Intermediate Current. This difference is attributed to the high vertical resolution of this model. This suggests that the model vertical resolution should be high in the equatorial region, where the high vertical mode motion dominates.

7. Summary

We conducted a numerical experiment with a global high-resolution model with 1/4 degrees horizontal resolution and 55 levels to investigate the role of meso-scale eddies on the general circulation and the mechanism of seasonal to interannual variability. The model simulated the separation of the Kuroshio and the equatorial currents system, which could not be represented in the previous models. This means that the model in this study is useful for the elucidation of the ocean circulation mechanism. We are now proceeding with the time integration of this model to spin up the circulation in the intermediate layer and water mass formation.

Acknowledgements

We would like to thank Director Otsuka and the members of the Scientific Computing Division for use of the super computer NEC SX-4 of the Japan Marine Science and Technology Center (JAMSTEC). Mr. Sasaki and the members of NEC helped us greatly in parallel computing. Mr. Hashimoto of Fuji Research Institute supported us in the visualization, and transplanting the MOM2 to the SX-4 system. The members of the Ocean Research Dept. of JAMSTEC constantly discussed this research with us. We express our gratitude to them. This work was supported by the funds of the Science and Technology Agency of the Japanese Government.

References

Arief, D. and S.P. Murray, 1996. Low-frequency fluctuations in the Indonesian throughflow through Lombok Strait, J. Geophys. Res., **101**, 12455-12464.

Bryan, K., 1969. A numerical method for the study of the circulation of the world ocean, J. Comput. Phys., **4**, 347-376.

Chelton, D.B. and M.G. Schlax, 1996. Global observations of oceanic Rossby Waves, Science, **272**, 234-238.

Cox, M.D., 1984. A primitive equation, 3-dimensional model of the ocean. GFDL Ocean Group Technical Report No. 1., Geophysical Fluid Dynamics Laboratory, Princeton, USA.

Fu, L.L. and R.D. Smith, 1996. Global ocean circulation from satellite altimetry and high-resolution computer simulation. Bull. Amer. Meteor. Soc., **77**, 2625-2636.

Godfrey, J.S., 1996. The effect of the Indonesian throughflow on ocean circulation and heat exchange with the atmosphere: A review, J. Geophys. Res., **101**, 12217-12237.

Halpern, D., 1987. Observations of annual and El Nin~ thermal and flow variations at 0°, 110°W and 0°, 95°W during 1980-1985, J. Geophys. Res., **92**, 8197-8212.

Hellerman, S. and M. Rosenstein, 1983. Normal monthly wind stress over the world ocean with error estimates, J. Phys. Oceanogr., **13**, 1093-1104.

Kuroda, Y. 1997. Variability of the currents off the north coast of New Guinea, to be submitted to J. Oceanogr.

Le Traon, P.Y., M.C. Rouquet and C. Boissier, 1990. Spatial scales of mesoscale variability in the North Atlantic as deduced from Geosat data, J. Geophys. Res., **95**, 20267-20285.

Legeckis, R., 1977. Long waves in the eastern equatorial Pacific; a view from a geostationary satellite, Science, **197**, 1177-1181.

Levitus, S., 1982. Climatological atlas of the world ocean, NOAA Prof. Pap No. 13, U.S. Govt. Print. Office, Washington, D.C., 173 pp.

Lukas, R., T. Yamagata, and J.P. McCreary, 1996. Pacific low-latitude western boundary currents and the Indonesian throughflow, J. Geophys. Res., **101**, 12209-12216.

Meyers, G., 1996. Variation of Indonesian throughflow and the El Nino - Southern Oscillation, J. Geophys. Res., **101**, 12255-12263.

Pacanowski, R., 1995. MOM 2 documentation user's guide and reference manual, Ver. 1.0, GFDL Ocean Group Technical Report No. 3, Geophysical Fluid Dynamics Laboratory, Princeton, USA.

Pacanowski, R. and S.G.H. Philander, 1981. Parametrization of vertical mixing in numerical models of tropical oceans, J. Phys. Oceanogr., **11**, 1443-1451.

Philander, S.G., 1989. El Nino, La Nina, and the Southern Oscillation, Academic Press, San Diego.

Richardson, P.L., 1983. Eddy kinetic energy in the North Atlantic Ocean from surface drifters, J. Geophys. Res., **88**, 4355-4367.

Sarmiento, J.L. and K. Bryan, 1982. An ocean transport model for the North Atlantic, J. Geophys. Res., **87**, 394-408.

Semtner, A.J., 1974. An oceanic general circulation model with bottom topography, Tech. Rep. **9**, 99 pp., Dep. of Meteorol., Univ. of Calif., Los Angeles.

Semtner, A.J. and R.M. Chervin, 1988. A simulation of the global ocean circulation with resolved eddies, J. Geophys. Res., **93**, 15502-15522.

Semtner, A.J. and R.M. Chervin, 1992. Ocean general circulation from a global eddy-resolving model, J. Geophys. Res., **97**, 5493-5550.

Smith, R.D., J.K. Dukowicz, and R.C. Malone, 1992. Parallel ocean general circulation modeling, Physica D, **60**, 38-61.

Stammer, D., R. Tokmakian, A. Semtner and C. Wunsch, 1996. How well does a 1/4° global circulation model simulate large-scale oceanic observations? J. Geophys. Res., **101**, 25779-25811.

Treguier, A.M., 1992. Kinetic energy analysis of an eddy resolving, primitive equation model of the North Atlantic. J. Geophys. Res., **97**, 687-701.

Wyrtki, K. and B. Kilonsky, 1984. Mean water and current structure during the Hawaii-to-Tahiti Shuttle Experiment, J. Phys. Oceanogr., **14**, 242-253.